Electronic Research Archive

http://www.aimspress.com/journal/ERA

ERA, 31(4): 2048–2070.
DOI: 10.3934/era.2023105
Received: 25 October 2022
Revised: 19 January 2023
Accepted: 06 February 2023
Published: 16 February 2023

Research article

Study on the storage stability performance enhancement mechanism of graphene on rubber-modified asphalt based on size effect

Yutong Xie, Yingli Gao*, Meijie Liao and Weiwei Tian

National Engineering Laboratory of Highway Maintenance Technology, Changsha University of Science & Technology, Changsha 410114, China

* **Correspondence:** Email: yingligao509@126.com; Tel: +18108458040.

Abstract: The application of waste rubber powder (WRP) for asphalt pavement could achieve the harmless and resourceful utilization of solid waste, but the storage stability of waste rubber powder modified asphalt (RA) is one of the main problems restricting its application. Existing studies have demonstrated that graphene could enhance the storage stability of RA, but graphene's size effect on the modifying effect and its corresponding mechanism are still uncertain. In this research, the effects of graphene microstructural properties (i.e., molecular size and layer number) on the storage stability of RA were investigated by storage stability testing, dynamic shear rheometry (DSR) testing and fluorescence microscopy (FM) testing, in combination with molecular dynamics simulation (MD). The experimental results indicated that graphene improved the storage stability of RA significantly, with few-layer graphene being more effective in enhancing it. MD was used to investigate the graphene size effect on RA in compatibility, intermolecular binding energy and structural stability of the system. The simulation results revealed that small-sized graphene molecules were more compatible with RA. Meanwhile, few-layer, small-sized graphene can provide higher binding energy and better enhancement of storage stability of RA. The number of graphene layers mainly influences the binding energy rather than solubility parameters. The relative concentration distribution results demonstrated that graphene facilitated the spatial distribution of asphaltenes, rubber components and light components. This research provides theoretical support for the rational selection of microstructural properties of graphene to improve the modified asphalt storage stability performance.

Keywords: waste rubber powder modified asphalt; graphene; storage stability; molecular dynamics; compatibility; size effect

1. Introduction

Waste rubber powder modified asphalt (RA) has excellent engineering performance in reducing driving noise, delaying reflective cracking, minimizing pavement water damage and withstanding heavy traffic [1,2]. In addition, RA has a significant role in improving the high temperature fatigue resistance and resistance to low temperature cracking of base asphalt [3]. As a polymer material which is hard to degrade by natural conditions, scrap tires can be used in road engineering after crushing to improve road performance and driving comfort [4,5]. At the same time, the harmless treatment and resource utilization of solid waste are realized to avoid "black pollution," which is aligned with the concept of green sustainable development and has good application prospects and environmental protection value [6,7]. However, the incompatibility of the rubber and base asphalt make them vulnerable to segregation during storage and transportation, which limits the application and further development of RA in engineering [8–11].

Nanomaterials are a common class of additives for enhancing the storage stability of RA. Graphene has shown excellent performance as an asphalt modifier. Wang et al. [12] evaluated the viability of adding carbon nanoparticles to asphalt binder. Softening point differences, rheological responses and micromorphology were tested, demonstrating that the carbon nanomaterial-modified asphalt was capable to satisfy the storage stability requirements. In accordance with Chen et al. [13], modified bitumen storage stability could be improved by the incorporation of graphene. Graphene enhances the viscoelasticity and the high- and low-temperature characteristics of RA, and it also increases the adhesion of ore and asphalt. Li et al. [14] discovered that the incorporation of nanoscale graphene to bitumen could remarkably increase the material's high-temperature resilience and temperature sensitivity, leading to improved thermal storage stability of modified bitumen. Singh et al. [15] analyzed the compatibility of graphene oxide (GO) rubber powder composite modified hot mix bitumen together with the structure and morphology of the modified bitumen. The results showed that WRP and GO were completely compatible with asphalt, offering better road performance. Meng et al. [16] discovered that the rheological and mechanical performances of RA incorporated with graphene were improved, with higher elastic recovery and deformation resistance. The phase distribution was also more uniform and continuous, resulting in improved storage stability and compatibility. Liu et al. [17] discovered that the doping of graphene and carbon black composites (GC) greatly enhanced the fatigue damage resistance and thermally activated healing characteristics of RA. Through physical and chemical interactions, the loose GC reacted with asphalt and formed tight connections. Ferrari et al. [18] demonstrated that an important indicator of graphene properties is the number of layers. From the above findings, it is clear that, as a new nanomaterial, graphene could improve the storage stability performance of RA. However, most existing studies mainly emphasized the reinforcement effect of graphene on RA. Although they can to some extent reflect the property changes and microscopic morphology of asphalt, the majority of them are simply phenomenological or qualitative descriptions, making it hard to clearly reveal the mechanism of the interaction between graphene and RA.

The properties of the material itself are impacted by the particle sizes, specific surface areas and other metrics that differ between various sizes and layers of graphene [19]. The characteristics of graphenes with different layers and their respective advantages in terms of performance and applications in emerging fields, such as novel energy materials, composites, biomaterials and sensors, have been summarized [20]. However, in the road materials field, there are insufficient

studies about graphene size effect on modified asphalt properties, which results in the inability to optimize the modification effect of graphene. Owing to advances in graphene preparation technology, it is now possible to produce graphene with specific layers and sizes. To better guide the design and development of graphene materials and achieve optimal asphalt performance enhancement when graphene is used as a modifier, it is necessary to explore further the effect of graphene microstructural properties on RA storage stability and the modification mechanism [21].

Molecular dynamics simulation (MD) characterizes the behavior of materials at an atomic or molecular level, especially to describe the structure-property relationships of materials, which could be used to explain the molecular motion behaviors of multiple components in modified asphalt [22]. At present, the modifying effect of graphene on RA storage stability still lacks quantitative explanation. Graphene/rubber composite modified asphalt (GRA) was taken as the research object. The interaction behavior in GRA and the graphene size effect on modified asphalt storage stability were studied by combining multiple-scale tests with MD.

In this paper, the graphene size effect on RA storage stability is discussed in combination with experimental analysis and MD. The influence of different graphene types in modified asphalt on the enhancement of storage stability was investigated from a macroscopic perspective using storage stability tests and dynamic shear rheometry (DSR) tests. The effect of different layers and sizes of graphene in GRA was explained from a microscopic perspective by fluorescence microscopy experiments (FM). Meanwhile, the size effect of graphene and its mechanism on the storage stability of GRA were investigated by MD for the application of graphene in modified asphalt.

2. Objective

This research uses multiple-scale experimental characterizations and molecular dynamics simulation to study the enhancement effect of graphene on RA storage stability. An emphasis was placed on how the geometric properties of graphene affected the modification effect.

3. Materials and methodology

3.1. Materials and preparation

3.1.1. Materials

AH-70 road asphalt was selected for this study, and the performance indices of the original asphalt used were examined based on the Chinese standard JTG E20-2011, as shown in Table 1. The waste rubber powder (WRP) was produced from whole automobile radial tires, with a fineness of 40 mesh. Natural rubber (NR), butadiene rubber (BR) and styrene-butadiene rubber (SBR) are the three major ingredients of the chosen WRP. The proportion of each component was NR: BR: SBR = 36.66: 8.88: 54.46% [23]. According to Chinese standards JT/T797-2011, GB/T 14837 and GB/T 3516, the technical indices of the measured WRP are listed in Table 2. Three types of graphene particles, e.g., single-layer graphene (SLG), few-layer graphene (FLG) and multi-layer graphene (MLG), were used in this study, and their performance indices are listed in Table 3.

Table 1. Basic performance indices for AH-70 asphalt.

Test index	Specification requirements	Specification	Tested data
Penetration (25℃, 5 s, 100 g) (0.1 mm)	60–80	T0604	70.7
Ductility (5 cm/min, 10 ℃) (cm)	≥ 15	T0605	41
Softening point (℃)	≥ 46	T0606	52.3
Viscosity, 135 ℃ (MPa·s)	-	T0625	530

Table 2. The basic indices of WRP.

Test index	Specification requirements	Specification	Tested data
Fiber content (%)	< 0.50	JT/T797-2011	0.16
Metal content (%)	< 0.01	JT/T797-2011	0.008
Rubber hydrocarbon content (%)	≥ 42	GB/T 14837	49.1
Carbon black (%)	≥ 28	GB/T 14837	31.3
Acetone extract content (%)	≤ 22	GB/T 3516	12.4

Table 3. Detection results of basic performance indices of graphene.

Graphene Species	SLG	FLG	MLG
Graphene layer number	1–2	3–5	6–10
Sheet diameter (μm)	6–12	8–14	10–16
Stack density (g/cm^3)	0.03–0.05	0.06–0.08	0.06–0.068
Carbon Content (%)	99	98	96

Using scanning electron microscopy (SEM) at a magnification of 7000, three different types of graphene were observed. Figure 1 depicts the apparent morphologies of these particles. SLG shows a thin sheet layer with a relatively smooth and flat surface. FLG films show a large number of folds on the surface, showing a silk-like appearance. MLG is multiple lamellar layers stacked together, with a rough surface and some protrusions. The results illustrated significant differences in the apparent morphologies of SLG, FLG and MLG.

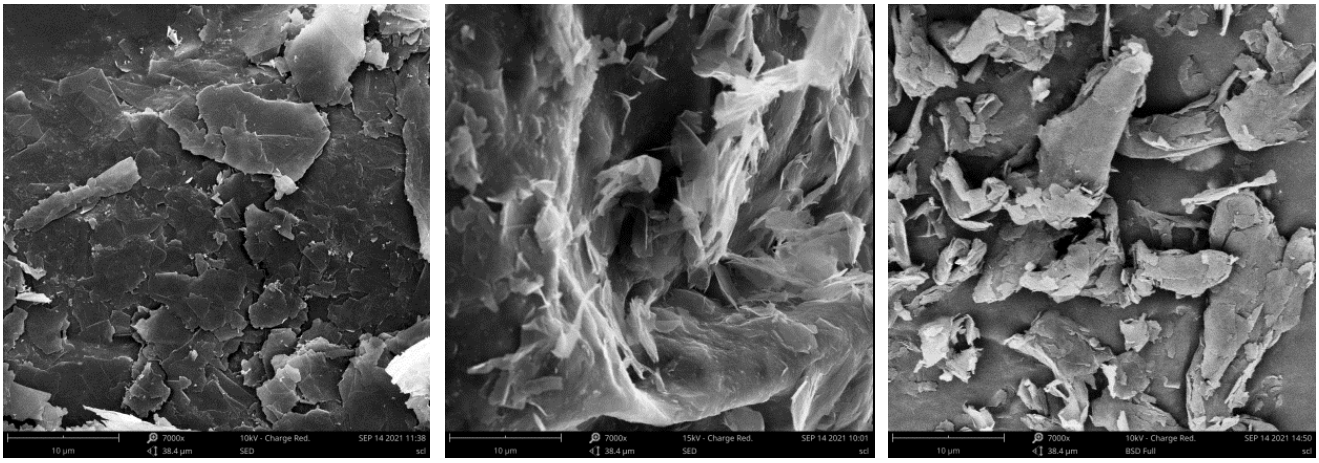

(a) (b) (c)

Figure 1. SEM images: (a) SLG, (b) FLG, (c) MLG.

3.1.2. Preparation of modified asphalt

First, an oven was used to melt the base asphalt. Next, the asphalt was transferred into a heating sleeve with the temperature set to 180 °C. When the asphalt temperature reached 175 ℃, low speed shearing was started at a shearing speed of 1000 r/min to eliminate air bubbles and prevent swelling after adding the WRP. Then, 20% pre-dried WRP and 5% ultrasonically dispersed graphene were gradually added while being stirred with a glass rod using the external blending method [24]. When 180 ℃ was reached, the shear speed was set to 4000 r/min for 50 minutes, and finally, the modified asphalt specimens were placed in a 175 ℃ oven for 45 minutes of continuous development. The preparation process is illustrated in Figure 2.

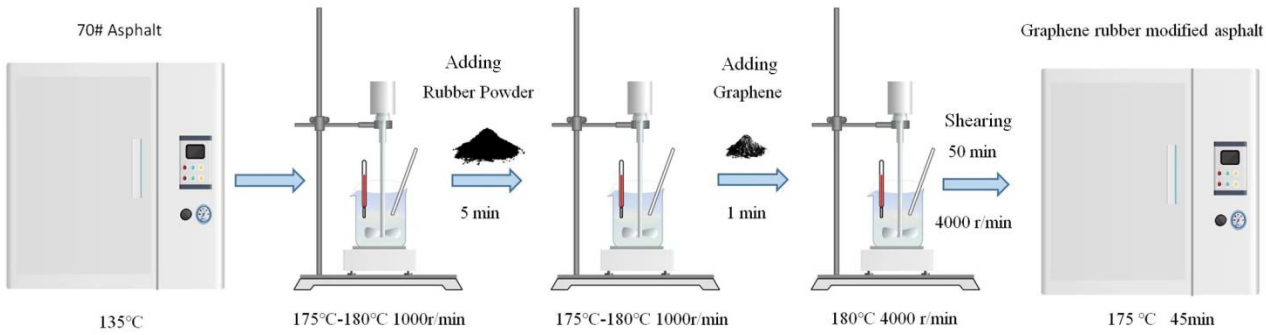

Figure 2. Preparation of graphene/rubber composite modified asphalt.

3.2. Property Tests

The flow chart of this work is illustrated in Figure 3.

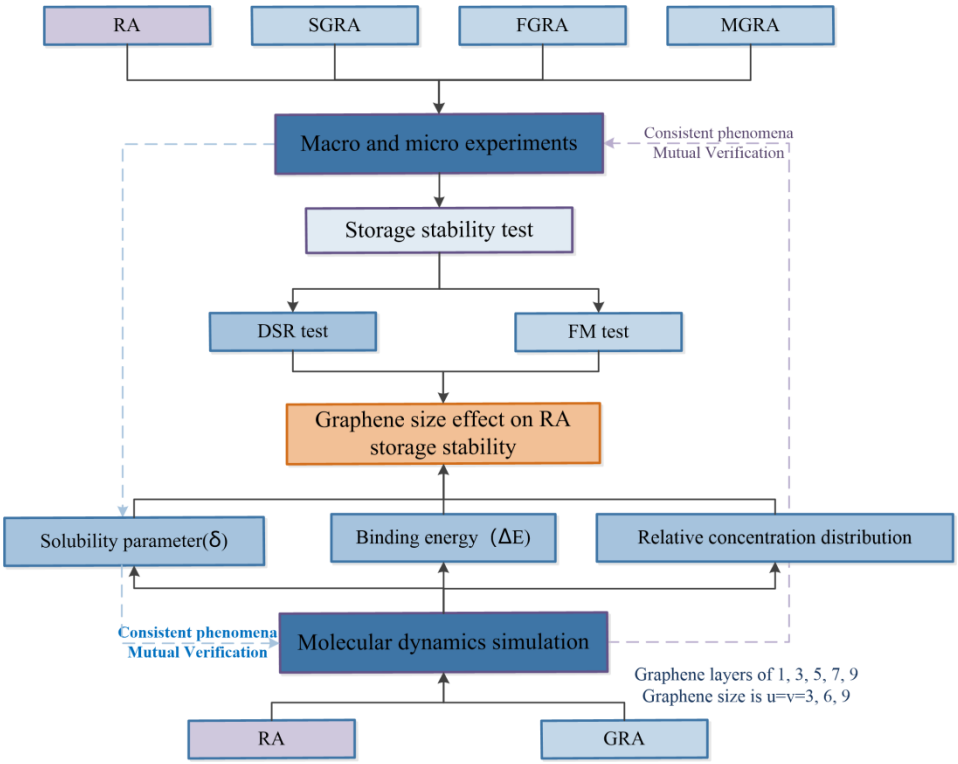

Figure 3. Experimental flowchart.

3.2.1. Storage stability test

According to the specification ASTM D7173, single-layer graphene-modified rubber asphalt (SGRA), few-layer graphene-modified rubber asphalt (FGRA), multi-layer graphene-modified rubber asphalt (MGRA) and RA were taken for 48 h storage stability testing. After curing, the material was cut into three equally divided segments, of which the upper and bottom two were taken for subsequent experiments. The 48 h storage stability test simulated the process of a binary mixture of asphalt-rich phase and polymer-rich phase dissociation under high-temperature storage in the mixing plant. The softening points of the specimens of different tube segments were evaluated and compared after sufficient mixing, and storage stability was indicated by softening point test (ASTM D36) and DSR test (ASTM D7175).

In accordance with ASTM D7175 and related literature [25,26], the separation ratios (R_S) under high-temperature and low-frequency conditions are reliable metrics to evaluate RA storage stability, followed by the percentage of separation (S_P). DSR tests were performed on samples from the upper and bottom segments of modified bitumen tubes after the storage stability experiments. Performing DSR at 58 °C, frequency sweep experiments were performed from 0.15 to 30 Hz. The dynamic shear modulus G* and phase angle δ of specimens at 0.15 and 1.5 Hz were selected to calculate R_S according to Eq (1) [25,27]. Using DSR's LAS-test mode, the oscillatory time sweep tests were performed at 10 rad/s and 58 °C, and the S_P was calculated according to Eq (2) [25,27].

$$R_S = \frac{(G^* / \sin\delta)_u}{(G^* / \sin\delta)_b} \tag{1}$$

$$S_P = \frac{Max(G_u^*, G_b^*) - G_{avg}^*}{G_{avg}^*} \times 100 \quad (2)$$

where u represents the upper specimen of test tubes, b represents the bottom specimen of test tubes, and avg indicates the average of the values taken for the upper and bottom segments.

3.2.2. Fluorescence microscopy experiments (FM)

Fluorescence microscopy experiments (FM) were performed using a German Leica DM-40 ortho-mounted fluorescence microscope with excitation wavelength of 470 ± 20 nm and emission sheet wavelength of 515 nm. The effects of different sizes and layers of graphene on the degree of separation from the asphalt phase of the polymer phase were investigated by comparing fluorescence microscopy images for the upper and bottom segments of the specimen after storage stability tests. The preparation process of fluorescence microscopy experimental specimens was the following: The asphalt specimen was heated to flow dynamics, and a drop of asphalt was taken onto the slide. Then, the slide was covered and pressed flat and thin until there was some light transmission. If the sample was too thick, it could be heated in the oven and pressed again until there was light transmission. The cooled specimen could be placed in a fluorescence microscope for observation.

3.3. Simulation models and methods

3.3.1. Modeling method

Molecular dynamics simulations were implemented using the COMPASSII force field of the Materials Studio (MS) software. The asphalt molecular models were constructed according to the chemical four-component method, using the AAA-1 model suggested by Li et al. [28]. Asphalt in the system is composed of 12 molecules. The number of each molecule of asphalt is determined according to the asphaltene, saturate, aromatic and resin contents measured by the four-component test (ASTM D4124). Molecular structures of twelve components of asphalt are illustrated in Figure 4. Numbers of the twelve molecules in the models are presented in Figure 5, and the ratios of four components in the models and experimentally obtained values are shown in Figure 6. Natural rubber (NR), butadiene rubber (BR) and styrene-butadiene rubber (SBR) are the three main ingredients of the WRP used [30]. The monomers cis-1,4-polybutadiene and cis-1,4-polyisoprene are polymerized to form the homopolymers NR and BR, respectively. SBR is a random copolymer primarily composed of trans-1,4-butadiene, 1,2-butadiene, styrene and cis-1,4-butadiene [23]. The structures of rubber molecules and their monomers are shown in Figure 7. In this study, graphene molecules with different combinations of layers and sizes were constructed. Selected layer numbers were 1, 3, 5, 7, 9, and the sizes were selected in supercell with three sizes of repeating monomer, u = v = 3, 6, 9, corresponding to edge lengths of 7.38, 14.76 and 22.14 Å, respectively. In Figure 8, the constructed graphene molecular models are shown.

Based on the above work, after Geometry Optimization of each molecule, the RA model and GRA models were constructed in the Amorphous Cell.

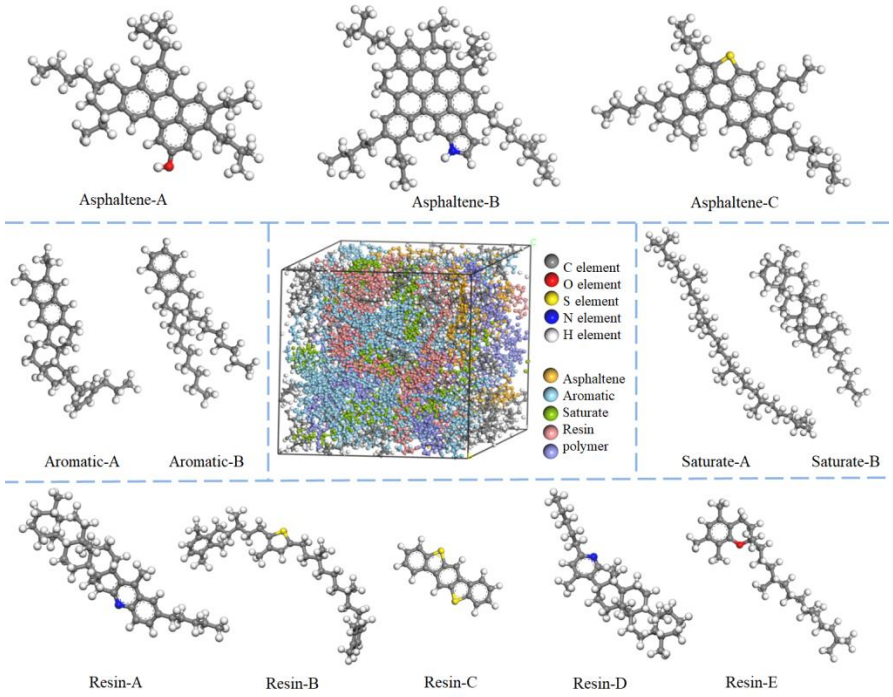

Figure 4. Molecular structures of AAA-1 asphalt systems.

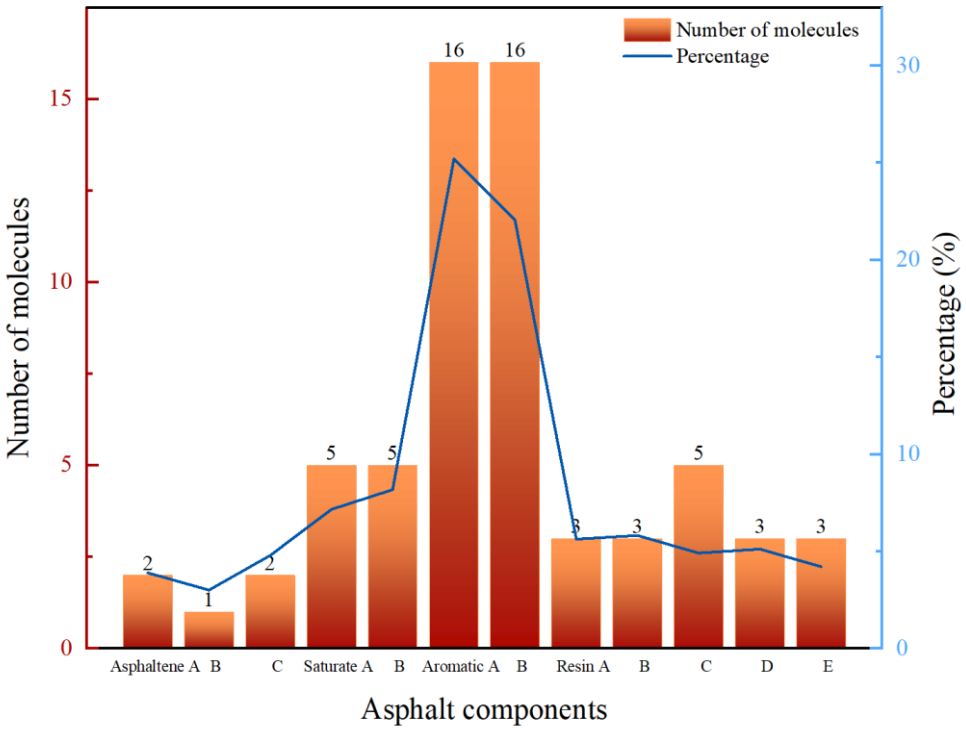

Figure 5. The molecular numbers of asphalt components in the models.

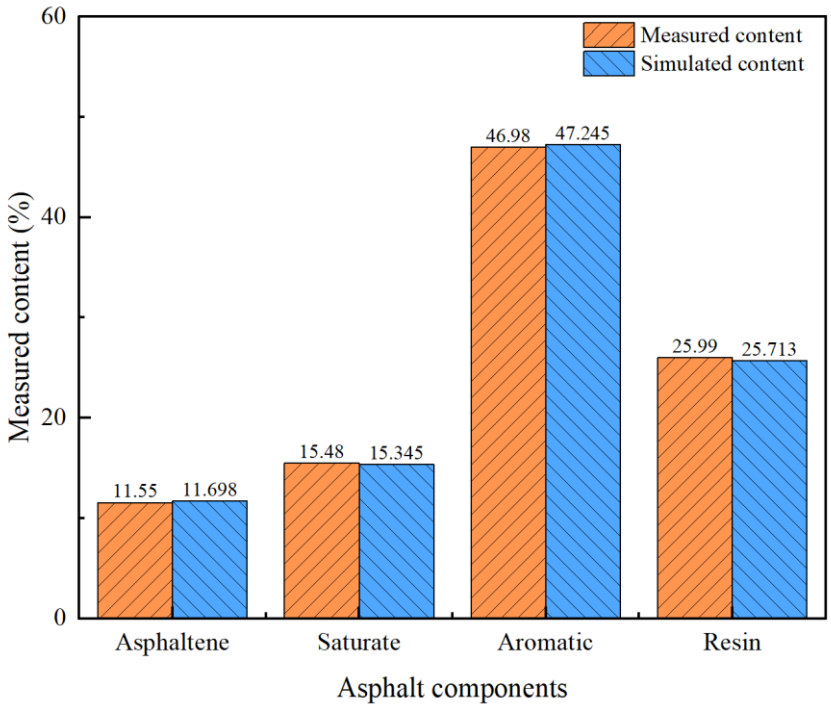

Figure 6. Four-component ratios of models and experiment.

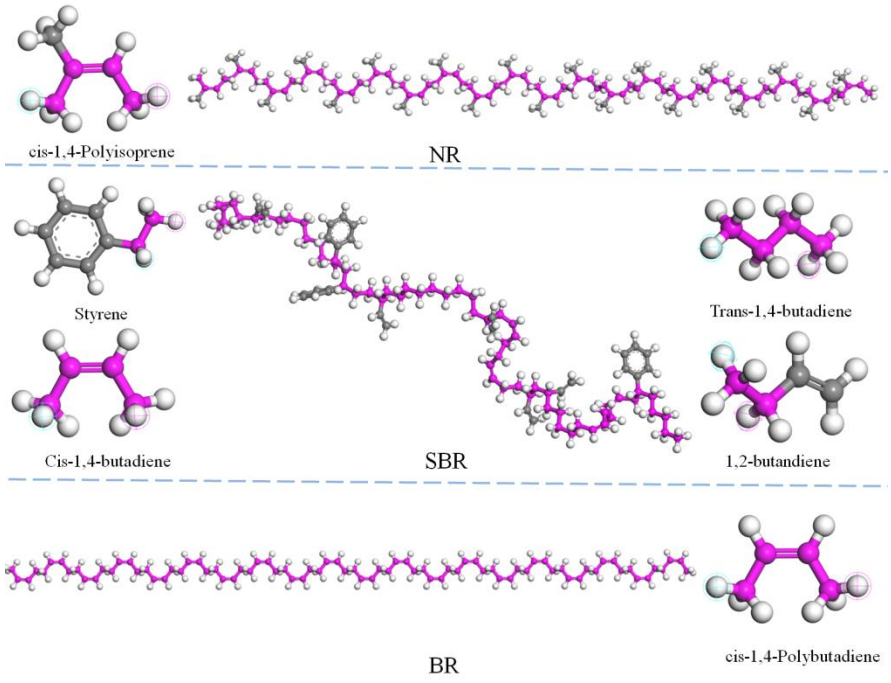

Figure 7. Molecular structure models of the constituents of WRP.

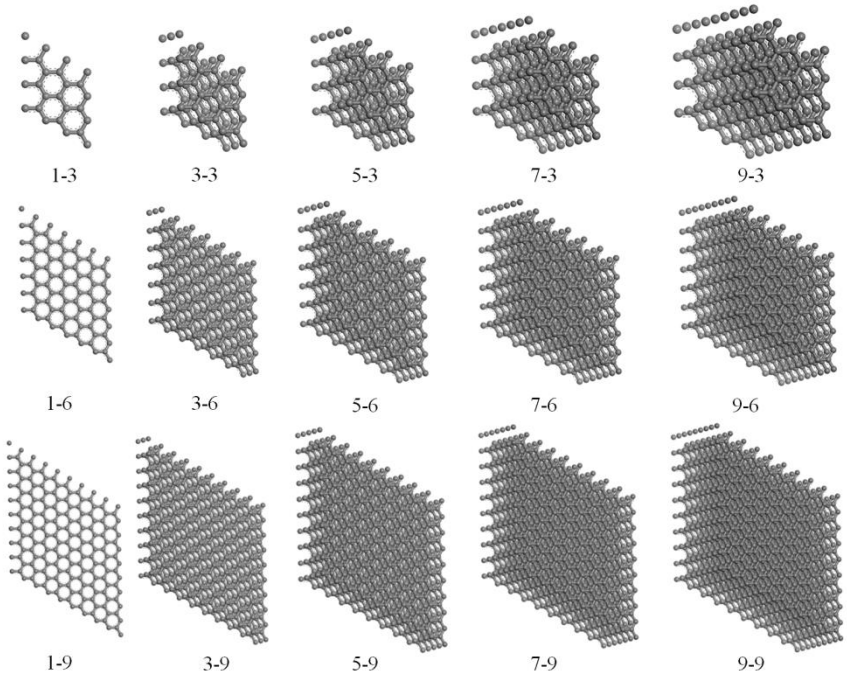

Figure 8. Molecular models of graphene with different numbers of layers and sizes.

3.3.2. Simulation method

Once the modified asphalt system model was completed, the geometry was first optimized in Forcite module until convergence conditions were met, and the Smart algorithm was chosen to find the lowest potential energy conformation. Then, to remove irrational energies from each model, asphalt molecules were annealed in the NPT ensemble (constant-pressure, constant-temperature) at 300 to 500 K and an atmospheric pressure of 1.01×10^{-4} GPa. The model was then sufficiently relaxed to reach the equilibrium state after 100,000 steps of dynamics simulations in the NVT ensemble (canonical ensemble). After completing molecular dynamics simulations for each asphalt system at 298 and 436 K with 0.2 fs time step and 100,000 steps of NPT ensemble, the obtained files were subjected to parametric calculations.

3.3.3. Model Verification

In a system, the normalized probability of a particle appearing radially around a reference particle at a given distance r is described by the radial distribution function (RDF) [29]. The trajectory file of each modified asphalt system model after dynamic simulation was operated by the Analysis function of MS to obtain the intramolecular RDF. In Figure 9, the RDFs of the constructed models show multiple peaks in the range of 0–4Å, which gradually become flat and converge to 1 after r > 5Å. This demonstrates that the constructed asphalt models are non-crystalline structures with remotely disordered and proximally ordered internal masses [30]. The presence of the peaks in RDF also reflects the fact that the type of interaction between non-bonded atoms in the asphalt models is mainly van der Waals forces and hydrogen bonding, which is in line with actual asphalt [30]. Figure 10 displays the evolution of system parameters throughout the MD. After the simulation ran for 25 ps, it

was evident that the asphalt model had almost reached equilibrium.

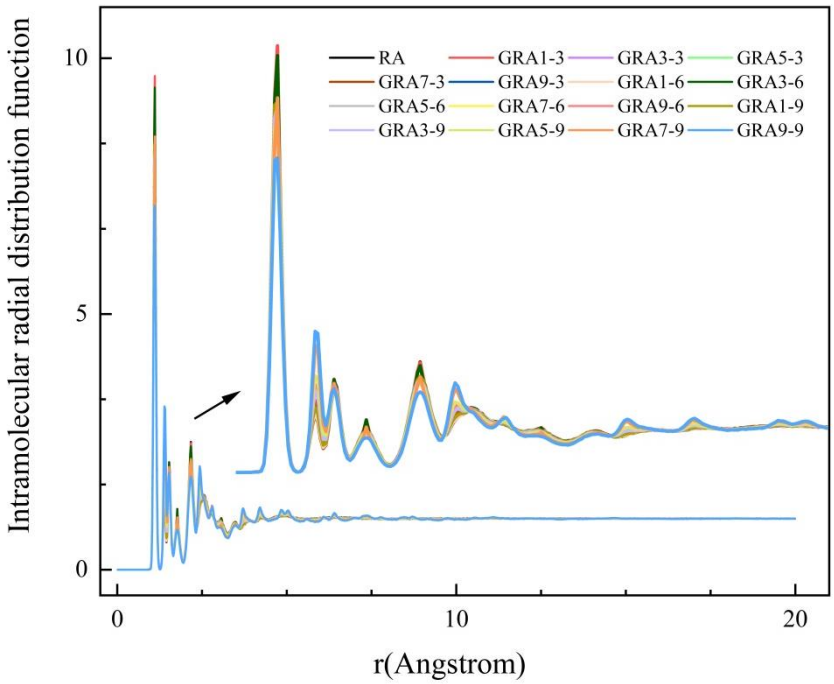

Figure 9. Radial distribution function (RDF) diagram.

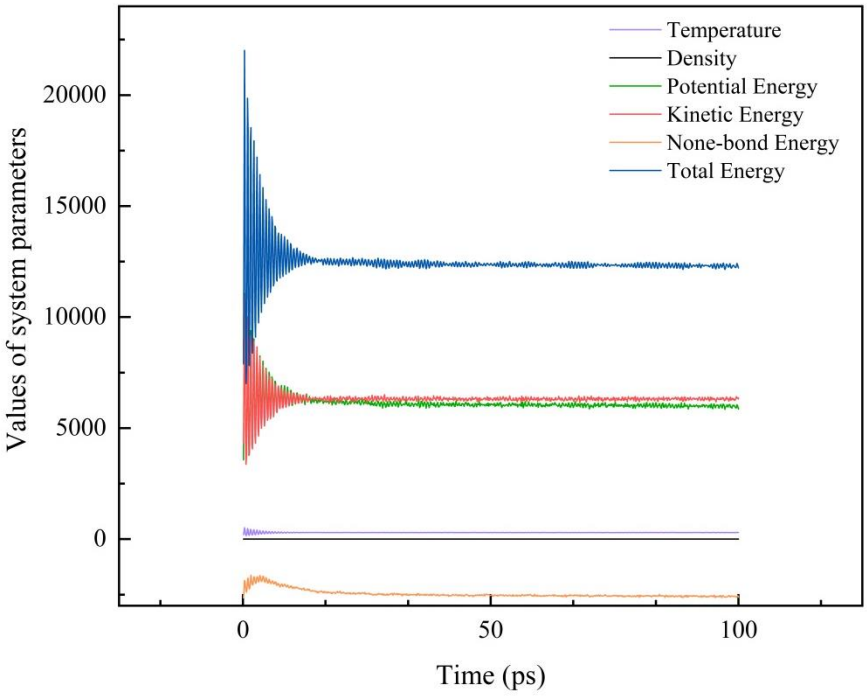

Figure 10. Molecular model system parameters variation.

4. Results and discussion

4.1. Multiple-scale experimental characterizations

4.1.1. Storage stability test results

The storage stabilities of the four modified asphalts were assessed by three indicators: softening point difference, R_S value and S_P value. After storage stability testing, segments at the upper and bottom parts of the tubes were tested for the softening point, the frequency sweep and the oscillatory time sweep of DSR. The results obtained are summarized in Table 4.

Softening point difference results revealed the values of SGRA, FGRA and MGRA were significantly smaller than that of RA. Compared to the RA, with a softening point difference of 4.2 °C, the decrease in GRA values ranged from 11.9 to 45.24%. The data revealed that doping with graphene could alleviate the phase separation of RA, with the most obvious improvement with FLG. The improvement effect on asphalt storage stability was FLG > SLG > MLG.

As the R_S value approaches the range of 0.8–1.2, the trend of separating the two phases of polymer-modified asphalt is less pronounced [25]. The R_S values of RA were 0.21 at 0.15 Hz frequency condition and 0.11 at 1.5 Hz frequency condition, which were apparently lower than the specified range, indicating that more severe phase separation occurred from RA in the thermal storage stability experiments. The SGRA, FGRA and MGRA all had significantly higher R_S values than those of RA, which proved that the incorporation of graphene enhanced the bonding of the polymer phase to the asphalt phase under thermal storage conditions. A similar conclusion can be obtained in the S_P results. The S_P values of SGRA, FGRA and MGRA were significantly lower than that of RA. Lower S_P values mean that the modified asphalt is less likely to segregate under thermal storage conditions. FGRA in 0.15 and 1.5 Hz frequency conditions can provide the desired R_S value of 0.8–1.2, and the S_P value of FGRA is the lowest among the four types of modified asphalt. These results suggest that FGRA is virtually free from phase separation and has significantly improved storage stability compared to RA. According to the analysis of R_S values, the improvement effect on asphalt storage stability was FLG > MLG > SLG. However, according to the analysis of S_P values, the improvement effect on asphalt storage stability was FLG > SLG > MLG.

From the above laboratory phenomena, FLG showed the best performance in improving RA storage stability. On the other hand, the enhancement efficiencies of SLG and MLG are different when different evaluation indices are adopted, so the graphene size and the number of layers will be further subdivided in subsequent segments.

Table 4. Parameter values for evaluating the modified asphalt storage stability.

Type of modified asphalt	RA	SGRA	FGRA	MGRA
Softening point difference	4.2	2.8	2.3	3.7
R_S (0.15 Hz)	0.21	0.63	0.88	0.68
R_S (1.5 Hz)	0.11	0.65	0.99	0.84
S_P	41.8	27.2	2.8	38.0

4.1.2. Fluorescence microscope

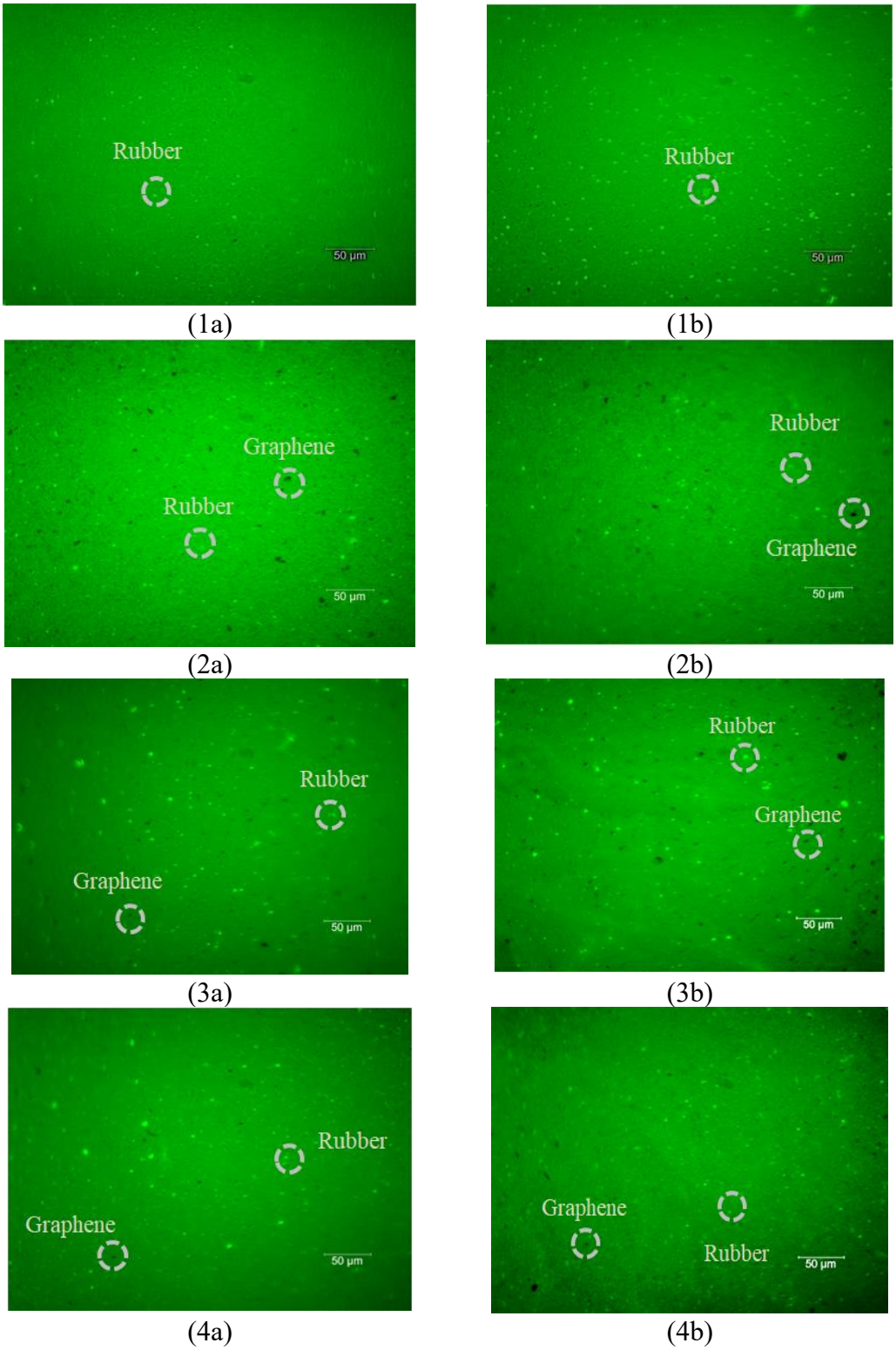

Figure 11. Fluorescence microscopy images of upper and bottom samples after storage stability test: (1a) RA upper sample, (1b) RA bottom sample, (2a) SGRA upper sample, (2b) SGRA bottom sample, (3a) FGRA upper sample, (3b) FGRA bottom sample, (4a) MGRA upper sample, (4b) MGRA bottom sample.

Samples of the upper and bottom segments of four modified asphalts were observed by fluorescence microscopy after storage stability tests. The distribution state of rubber powders in asphalt after a long storage time visually reflects the separation characteristics of the polymer phase and asphalt phase. The images are shown in Figure 11. The fluorescent spots in the images obtained by the fluorescence microscope were counted using ImageJ software, and the difference in the number of fluorescent spots between the upper and bottom segments of each specimen was calculated, with the results shown in Figure 12.

The polymer in RA was distributed in particle form in the continuous phase of the asphalt. As shown in Figure 11 (1a),(1b), the rubber powder particles at the upper part of the RA were fewer than at the bottom segments, indicating obvious segregation inside. In the images of SGRA, FGRA and MGRA, the fluorescence spots difference between the upper and bottom segments is small. From Figure 12, the differences in the number of fluorescent spots in the upper and bottom two segments of SGRA, FGRA and MGRA decreased by 78.5, 87.9 and 75.8%, respectively, compared with RA, indicating that the incorporation of graphene obviously reduced the phase separation in GRA.

A possible reason for segregation in RA is that the asphalt viscosity has decreased under thermal storage conditions, and the network of polymer-asphalt linkage partially fails, making the binding effect on the rubber powder in the system smaller [31]. Graphene, with its large surface area, acts as a physical cross-link from rubber to asphalt and promotes bonding between them to limit the movement of asphalt molecules under thermal storage conditions, thus improving the storage stability of RA [32,33]. Graphene particles of different sizes and layers have different physical and surface chemical properties, which have different degrees of enhancing effects on the storage stability performance of RA.

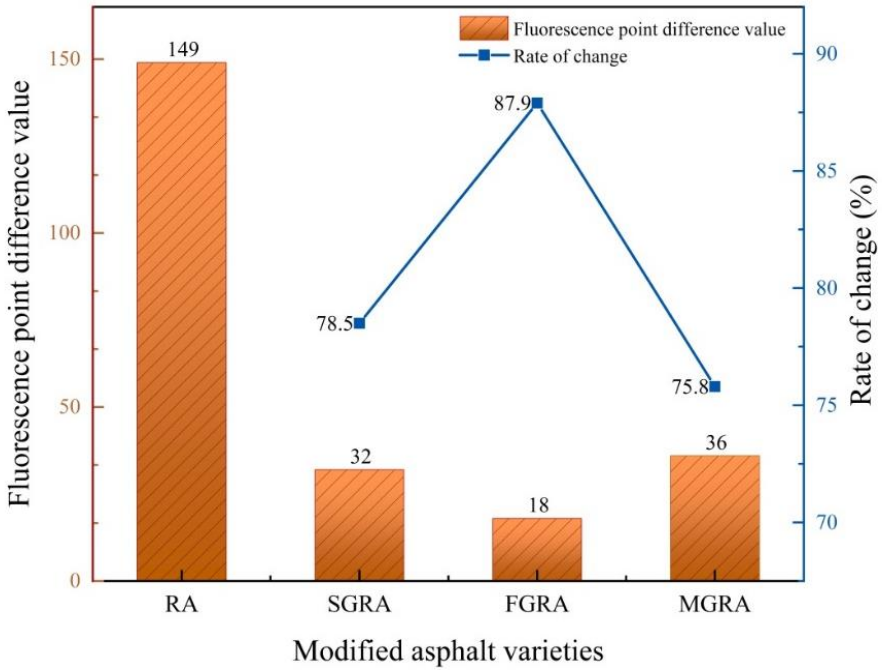

Figure 12. Difference in fluorescence points between the upper and bottom fluorescence images of the specimens.

4.2. Molecular dynamics simulation results

4.2.1. Solubility parameter (δ)

According to the theory of mixing heat of polymer blends, the cohesive energy density (CED) is the energy needed to counteract the intermolecular forces for 1 mol of cohesion in a unit volume, and the open square of the CED is the solubility parameter (δ) [34,35]. Solubility parameters are used to gauge the compatibility between materials. The tendency of segregation decreases as the solubility parameter difference ($\Delta\delta$) between the materials decreases [36]. It is calculated as follows:

$$\delta = \sqrt{E_{coh} / V} \tag{3}$$

where E_{coh} is the condensed matter cohesion energy, and V is the molar volume.

The solubility parameters obtained from the simulations are shown in Figure 13. The $\Delta\delta$ between RA and graphene can indicate the compatibility between those two phases, and good compatibility is possible when $\Delta\delta \leq 4.10$ $(J/cm^3)^{1/2}$ [36]. As shown in Figure 13, with the graphene size of u = v = 3, the solubility difference falls in the range of 2.4–2.7 $(J/cm^3)^{1/2}$ at 298 K and in the range of -0.2–0.1 $(J/cm^3)^{1/2}$ at 436 K. These values satisfy the condition that $\Delta\delta \leq 4.10$ $(J/cm^3)^{1/2}$, indicating that small-sized graphene molecules (u = v = 3) are well compatible with RA. At high temperatures, the solubility difference reduces and almost equals to zero, indicating that the increased temperature could avoid the precipitation of graphene due to incompatibility. If the compatibility between asphalt and graphene is poor, some graphene outside the network structure will fail to provide reinforcement due to stress concentration caused by agglomeration [37,38].

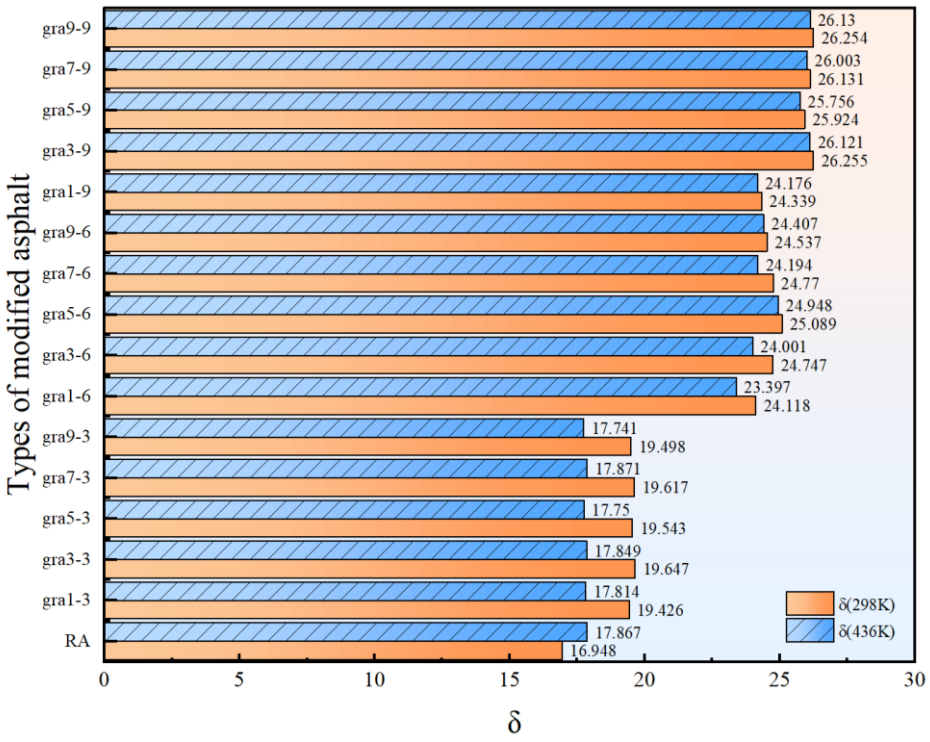

Figure 13. Solubility parameters (δ) of RA and different types of graphene.

As graphene size increases, the solubility of graphene molecules increases greatly. Therefore, the difference in solubility between graphene and RA shows an increasing trend, indicating the worsening compatibility between RA and graphene. When compared with the influence of the molecular size, the variation in layer number has relatively little impact on solubility parameters. Overall, the results indicate that small-sized graphene is more compatible with RA, and the solubility parameters are more related to the change in graphene size rather than its layers.

4.2.2. Binding energy（ΔE）

Based on the theory of weak intermolecular interactions, the final frame of the MD trajectory is selected to calculate the binding energy (ΔE) of graphene molecules with different combinations of layers and sizes in GRA system models [39]. A bound system maintains its integrity by having a system energy that is lower than the total energy of its components. The process of breaking this bound state requires energy absorption, and the more energy that is required, i.e., the larger the absolute value of ΔE is, the more stable the system will be when it is bound [40]. The ΔE values at 298 and 436 K were used to evaluate the association properties of graphene and RA at the interface under normal temperature and thermal storage conditions. The calculation of ΔE is given in Eq (4).

$$\Delta E = E_{(RA-Graphene)} - E_{(RA)} - E_{(Graphene)} \tag{4}$$

where ΔE represents the binding energy between graphene and RA, $E_{(RA\text{-}Graphene)}$ represents the energy of graphene rubber composite modified asphalt, $E_{(RA)}$ represents RA's energy, and $E_{(Graphene)}$ represents graphene's energy.

The ΔE values of different sizes and layers of graphene in the GRA models are listed in Table 5. The binding energy exhibits negative values (i.e., $\Delta E < 0$) in all models. This indicates that the components in graphene and RA are mutually attracted and that the doping of graphene enhances the stability of the combined asphalt phase and polymer phase [40].

Table 5. Binding energy (ΔE) of graphene molecules in modified asphalt (kcal/mol).

layers / sizes	1		3		5		7		9	
	298 K	436 K	298 K	436 K	298 K	436 K	298 K	436 K	298 K	436 K
3	11.0	15.0	83.1	86.7	77.6	84.7	74.8	77.6	72.6	77.0
6	31.1	104.0	198.5	208.2	288.3	222.7	363.7	341.4	429.8	381.8
9	247.2	196.9	366.7	343.8	552.8	516.2	625.7	622.4	726.7	687.1

According to the data in Table 5, graphene with the same number of layers shows an increasing trend of ΔE as the size increases. This may be because, as the size becomes larger, the contact area with surrounding components increases, with the contact surface being more prone to twisting and folding, thus increasing the roughness. The layered graphene structure forms an intercalation structure with the chain structure of saturated molecules, which has stable physical cross-linking and improves the thermal storage stability between asphalt and polymer [41]. For graphene molecules of size u = v = 6 and u = v = 9, ΔE tends to rise with increasing number of layers. When the size is

same, the FLG and MLG molecules can produce slip between the layers to increase the contact area with surrounding molecules [20], and the intercalation structure formed easily with the surrounding molecules improves the intermolecular binding energy and forms a graphene-asphalt-polymer association network [32,33].

However, only small-sized graphene (u = v = 3) can provide the desired compatibility between RA and graphene. Therefore, the binding energy was further characterized for the series with the size of u = v = 3. Regarding the effect of graphene layers, the ΔE of RA and graphene with increasing layers shows an increasing and then decreasing trend. Meanwhile, FLG and MLG provide notably higher binding energies than SLG. For FLG, its small size has good compatibility with asphalt. Also, its interlayer slip and fold increase the contact surface area and roughness, thus enhancing the intermolecular interaction force [20]. The highest binding energy for a layer number of 3 in molecular simulation results is consistent with the macroscopic experiments, where FLG has the best effect on the improvement of the storage stability of RA. The lower binding energy provided by the small-sized graphene with 5–9 layers is consistent with the slightly lower effect of MLG on improving storage stability than FLG in macroscopic experiments. This might be associated with the fact that graphene with 3 to 4 layers is more inclined to undergo interlamellar slippage, which was discovered by Gong et al. [42].

Overall, based on the balance between compatibility and binding energy, the simulation results point out that graphene molecules with size u = v = 3 and layer number of 3 layers have the best modification effect on RA storage stability.

4.2.3. Relative concentration distribution

The relative concentration distribution (RCD) of asphaltenes, light components and rubber components in the model at 436 K was obtained in the Forcite module. Based on the theory of colloidal structure, colloids are composed of micelles formed by resins adsorbed around asphalt as dispersions, dispersed in a dispersion medium consisting of saturates and aromatics, and swollen rubber powders are dispersed in asphalt. Homogeneous dispersion of the asphaltenes leads to a stable colloidal structure through interaction with lighter components [43]. Graphene has a similar morphology to asphaltene, and it can act as a nucleus for the asphaltic micelles when dispersed in the asphaltic colloid [12]. This could enhance the link between the polymer and asphalt phases, reducing the possibility of segregation. Its excellent thermal conductivity also facilitates rapid and homogeneous dispersion of bitumen for heat transfer, thus improving the high temperature rheology of bitumen [37,38]. Based on the above findings, the GRA model of graphene with a layer number of 3 and a size of u = v = 3 was chosen to analyze the RCD of constituents and compared with the results of the RA model. Figure 14 shows the distribution of the constituents in the RA and GRA models. Figure 15 shows the RCDs of asphaltenes, light components and rubber powder molecules in the directions of the X, Y and Z coordinate axes in the RA and GRA models.

As can be seen from Figure 14, asphaltene dispersion of the GRA model is more uniform than that of the RA model. As shown in Figure 15(a),(b), both in the RA and GRA models, there are multiple asphaltene peaks in the triaxial directions. However, more asphaltene peaks appear in the GRA model, and these peaks are lower and uniformly distributed throughout the model cross-section, indicating a more uniform asphaltene dispersion in the system with graphene, which is consistent with the direct observation of the model. From Figure 15(c),(d), the light components in

the GRA model have more peaks and fewer peak fluctuations compared to those in the RA model, and they are more uniformly distributed in all three directions. From Figure 15(e),(f), the rubber components have obvious peaks in all three directions in the GRA model, the peaks are higher, and the polymer phase is more aggregated, which is consistent with the molecular distribution characteristics of rubber powder in the GRA model in Figure 14 [39].

Comparing Figure 15(a),(e), it can be found that the asphaltene peaks and the rubber components peaks in the RA model have a slight overlap and close distance in triaxial directions. In contrast, in the GRA model as illustrated in Figure 15(b),(f), the asphaltene peaks do not overlap with the rubber component peaks. Moreover, the asphaltene peaks appear at the trough of the RCD curve of the rubber components. This indicates that both asphaltenes and rubber molecules are dispersed in the light components, which facilitates the spatial distribution of rubber molecules to absorb the light components and dissolve them. This strengthens the weak interface of asphalt and WRP, increasing the cohesion of RA and improving storage stability [39].

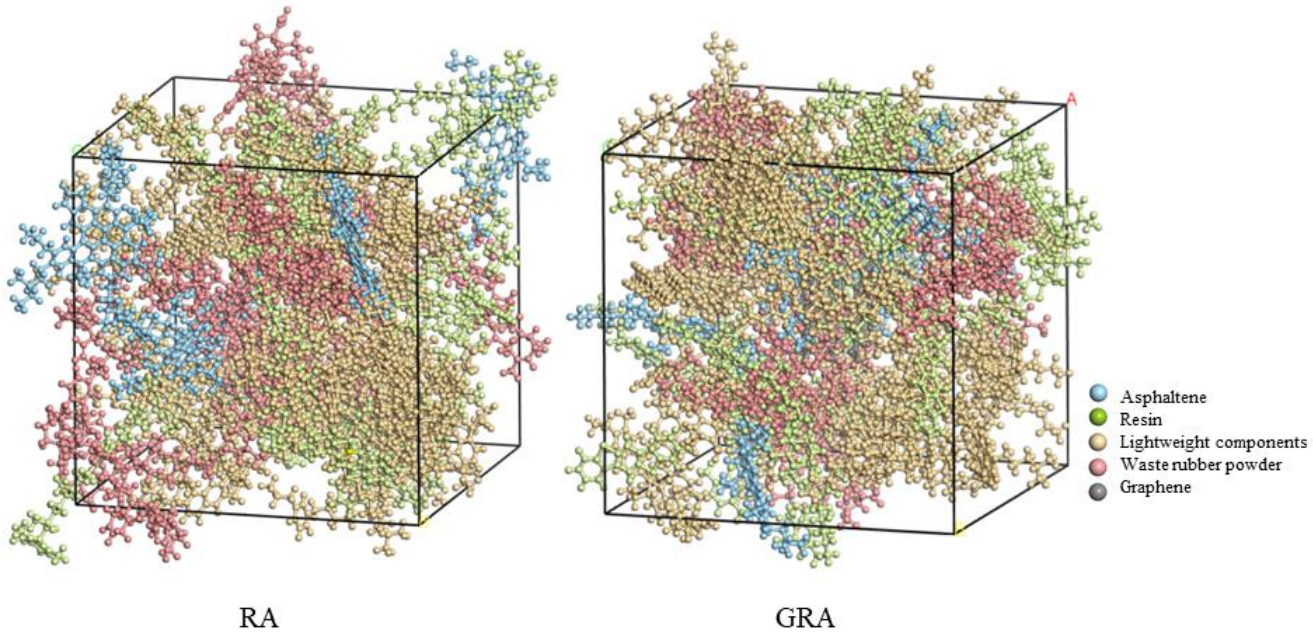

Figure 14. Distributions of components in RA and GRA.

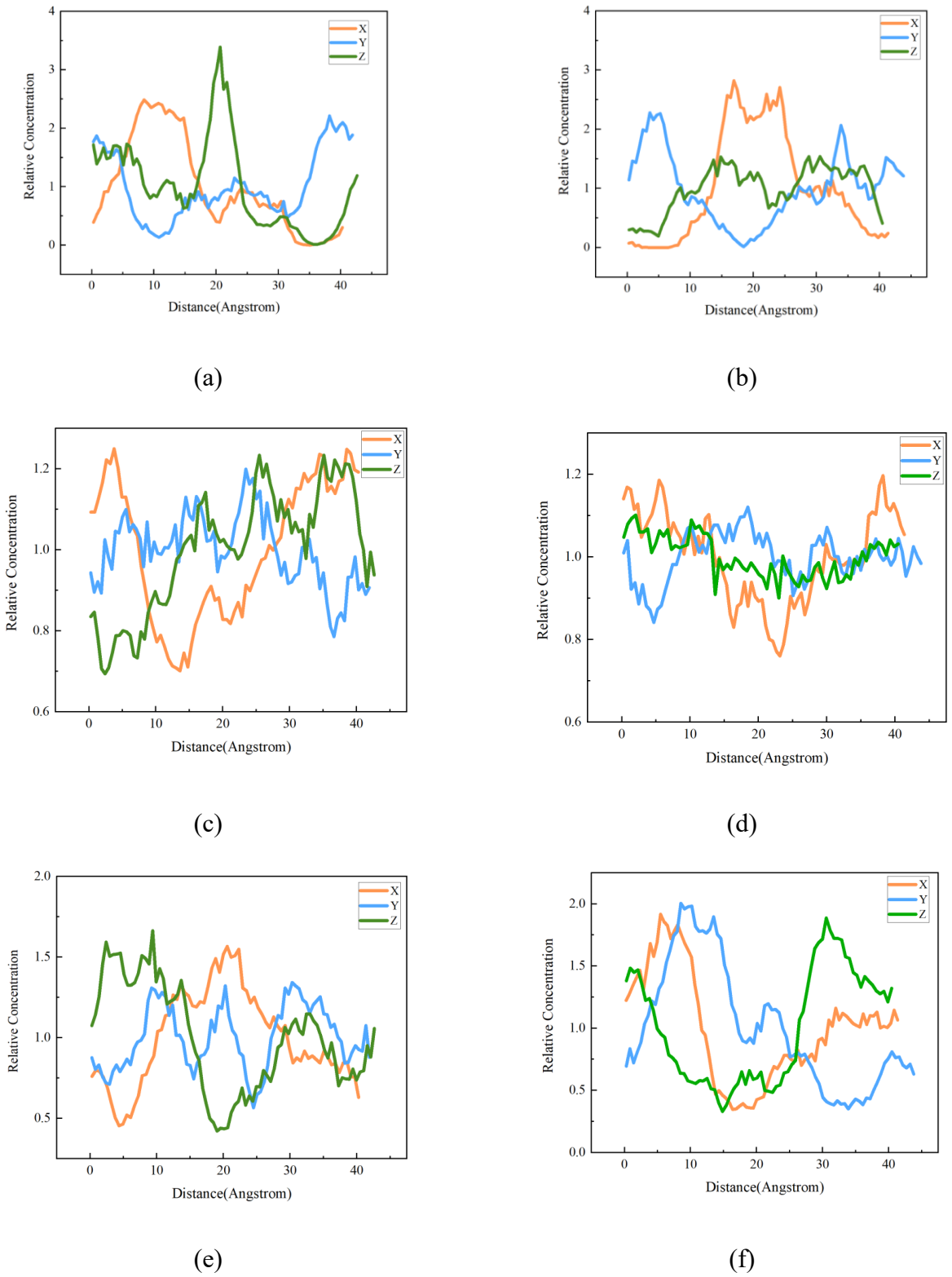

Figure 15. Relative concentration distributions: (a) Asphaltenes in RA model, (b) Asphaltenes in GRA model, (c) Light components in RA model, (d) Light components in GRA model, (e) Rubber components in RA model, (f) Rubber components in GRA model.

5. Conclusions

To investigate the graphene size effect on the storage stability of RA and explore the better application and development direction of graphene in modified asphalt, this research combined macro and micro experiments and MD to reach the following conclusions:

1) The storage stability test and DSR results indicated that graphene could enhance the storage stability of RA, with FLG being the most effective in improving the phase separation that exists in RA at high temperature storage conditions.

2) The fluorescence microscopy experiment indicated that graphene could promote the bonding of rubber and asphalt and prevent the partial failure of polymer-asphalt connection network during thermal storage, thus improving the stability of RA. In addition, GRA doped with few-layer graphene has a superior microstructure, which is in line with the conclusions obtained from macroscopic experiments.

3) The molecular dynamics simulation indicated that graphene with a layer number of 3 and a size of u = v = 3 was the most effective in enhancing the storage stability of RA. Graphene layer number mainly influences the binding energy, while the graphene size primarily dominates both solubility parameters and binding energy.

4) The $\Delta\delta$ and ΔE results indicated that both $\Delta\delta$ and ΔE between RA and graphene increase as the graphene size increases, indicating a decrease in compatibility and an increase in binding energy. For GRA models with graphene sizes of 6 and 9, ΔE rises with increasing number of layers, while for GRA models with graphene size of 3, an optimal layer number exists to ensure a lower $\Delta\delta$ and a higher ΔE.

5) The results of the relative concentration distributions support that the presence of graphene is conducive to the spatial distribution of asphaltene, rubber powder and light components, as well as the enhancement of the weak interfaces of asphalt and rubber powder.

Acknowledgments

Authors gratefully acknowledge the financial support from the National Natural Science Foundation of China (52278239 and 51978080), Key Research and Development Project of Hunan Provincial Science and Technology Department (2021SK2044) and Changsha University of Science & Technology Graduate Student Research Innovation Program (CX2021SS114).

Conflict of interest

The authors declare there is no conflict of interest.

References

1. Q. Z. Wang, N. N. Wang, M. L. Tseng, Y. M. Huang, N. L. Li, Waste tire recycling assessment: Road application potential and carbon emissions reduction analysis of crumb rubber modified asphalt in China, *J. Clean. Prod.*, **249** (2020), 119411. https://doi.org/10.1016/j.jclepro.2019.119411

2. T. Ma, H. Wang, L. He, Y. Zhao, X. Huang, J. Chen, Property characterization of asphalt binders and mixtures modified by different crumb rubbers, *J. Mater. Civ. Eng.*, **29** (2017), 04017036. https://doi.org/10.1061/(asce)mt.1943-5533.0001890
3. X. Ding, L. Chen, T. Ma, H. Ma, L. Gu, T. Chen, et al., Laboratory investigation of the recycled asphalt concrete with stable crumb rubber asphalt binder, *Constr. Build. Mater.*, **203** (2019), 552–557. https://doi.org/10.1016/j.conbuildmat.2019.01.114
4. F. Chen, J. Qian, Studies of the thermal degradation of waste rubber, *Waste Manage.*, (2003), 463–467. https://doi.org/10.1016/S0956-053X(03)00090-4
5. Y. Zhu, G. Xu, T. Ma, J. Fan, S. Li, Performances of rubber asphalt with middle/high content of waste tire crumb rubber, *Constr. Build. Mater.*, **335** (2022), 127488. https://doi.org/10.1016/j.conbuildmat.2022.127488
6. J. Li, M. Saberian, B. T. Nguyen, Effect of crumb rubber on the mechanical properties of crushed recycled pavement materials, *J. Environ. Manage.*, **218** (2018), 291–299. https://doi.org/10.1016/j.jenvman.2018.04.062
7. B. Świeczko-Żurek, P. Jaskula, J. A. Ejsmont, A. Kędzierska, P. Czajkowski, Rolling resistance and tyre/road noise on rubberised asphalt pavement in Poland, *Road Mater. Pavement Des.*, **18** (2017), 151–167. https://doi.org/10.1080/14680629.2016.1159245
8. F. J. Navarro, P. Partal, F. Martínez-Boza, C. Gallegos, Thermo-rheological behaviour and storage stability of ground tire rubber-modified bitumens, *Fuel*, (2004), 2041–2049. https://doi.org/10.1016/j.fuel.2004.04.003
9. I. Gawel, R. Stepkowski, F. Czechowski, Molecular interactions between rubber and asphalt, *Ind. Eng. Chem. Res.*, **45** (2006), 3044–3049. https://doi.org/10.1021/ie050905r
10. H. Xue, Y. Cao, Q. Liu, H. Zhang, M. Zhang, Stability evaluation and mechanism of asphalts modified with various rubber powder contents, *Front. Mater.*, **7** (2021), 622479. https://doi.org/10.3389/fmats.2020.622479
11. P. Kong, G. Xu, J. Yang, X. Chen, Y. Zhu, Study on storage stability of activated reclaimed rubber powder modified asphalt, *Materials (Basel)*, **14** (2021), 4684–4684. https://doi.org/10.3390/ma14164684
12. R. Wang, Y. Xiong, M. Yue, M. Hao, J. Yue, Investigating the effectiveness of carbon nanomaterials on asphalt binders from hot storage stability, thermodynamics, and mechanism perspectives, *J. Clean. Prod.*, **276** (2020), 124180. https://doi.org/10.1016/j.jclepro.2020.124180
13. Y. Chen, Q. Wang, Z. Li, S. Ding, Rhysiological properties of graphene nanoplatelets/rubber crowd composite modified asphalt, *Constr. Build. Mater.*, **261** (2020), 120505. https://doi.org/10.1016/j.conbuildmat.2020.120505
14. X. Li, Y. M. Wang, Y. L. Wu, H. R. Wang, M. Chen, H. D. Sun, et al., Properties and modification mechanism of asphalt with graphene as modifier, *Constr. Build. Mater.*, **272** (2021), 121919. https://doi.org/10.1016/j.conbuildmat.2020.121919
15. B. B. Singh, F. Mohanty, S. S. Das, S. K. Swain, Graphene sandwiched crumb rubber dispersed hot mix asphalt, *J. Traffic Transp. Eng. (English Ed.)*, **7** (2020), 652–667. https://doi.org/10.1016/j.jtte.2019.02.003
16. Y. Meng, H. Guo, R. Xu, R. Zhang, C. Ma, Rheological and microscopic properties of graphene rubber composite modified asphalt, *Jianzhu Cailiao Xuebao/Journal Build. Mater.*, **23** (2020), 1246–1251. https://doi.org/10.3969/j.issn.1007-9629.2020.05.034

17. J. Liu, P. Hao, Z. Dou, J. Wang, L. Ma, Rheological, healing and microstructural properties of unmodified and crumb rubber modified asphalt incorporated with graphene/carbon black composite, *Constr. Build. Mater.*, **305** (2021), 124512. https://doi.org/10.1016/j.conbuildmat.2021.124512
18. A. C. Ferrari, J. C. Meyer, V. Scardaci, C. Casiraghi, M. Lazzeri, F. Mauri, et al., Raman spectrum of graphene and graphene layers, *Phys. Rev. Lett.*, **97** (2006), 187401. https://doi.org/10.1103/PhysRevLett.97.187401
19. S. K. Tiwari, S. Sahoo, N. Wang, A. Huczko, Graphene research and their outputs: Status and prospect, *J. Sci. Adv. Mater. Devices.*, **5** (2020), 10–29. https://doi.org/10.1016/j.jsamd.2020.01.006
20. Y. B. Xie, M. R. Huang, X. G. Li, Review: Layer-number controllable preparation of high-quality graphene for wide applications, *J. Harbin Inst. Technol. (New Ser.*, **27** (2020), 136–157. https://doi.org/10.11916/j.issn.1005-9113.20003
21. A. A. MOOSA, M. S. ABED, Graphene preparation and graphite exfoliation, *Turkish J. Chem.*, **45** (2021), 493–519. https://doi.org/10.3906/kim-2101-19
22. K. Vollmayr-Lee, Introduction to molecular dynamics simulations, *Am. J. Phys.*, **88** (2020), 401–422. https://doi.org/10.1119/10.0000654
23. F. Guo, J. Zhang, J. Pei, B. Zhou, Z. Hu, Study on the mechanical properties of rubber asphalt by molecular dynamics simulation, *J. Mol. Model.*, **25** (2019), 365. https://doi.org/10.1007/s00894-019-4250-x
24. Y. Chen, Q. Wang, Z. Li, S. Ding, Rhysiological properties of graphene nanoplatelets/rubber crowd composite modified asphalt, *Constr. Build. Mater.*, **261** (2020), 120505. https://doi.org/10.1016/j.conbuildmat.2020.12050-5
25. Y. Wen, Q. Liu, L. Chen, J. Pei, J. Zhang, R. Li, Review and comparison of methods to assess the storage stability of terminal blend rubberized asphalt binders, *Constr. Build. Mater.*, **258** (2020), 119586. https://doi.org/10.1016/j.conbuildmat.2020.119586
26. G. Polacco, S. Filippi, F. Merusi, G. Stastna, A review of the fundamentals of polymer-modified asphalts: Asphalt/polymer interactions and principles of compatibility, *Adv. Colloid Interface Sci.*, **224** (2015), 72112. https://doi.org/10.1016/j.cis.2015.07.010
27. M. Ragab, M. Abdelrahman, Enhancing the crumb rubber modified asphalt's storage stability through the control of its internal network structure, *Int. J. Pavement Res. Technol.*, **11** (2018), 13–27. https://doi.org/10.1016/j.ijprt.2017.08.003
28. D. D. Li, M. L. Greenfield, Chemical compositions of improved model asphalt systems for molecular simulations, *Fuel*, **115** (2014), 347–356. https://doi.org/10.1016/j.fuel.2013.07.012
29. G. Xu, H. Wang, Molecular dynamics study of oxidative aging effect on asphalt binder properties, *Fuel*, **188** (2017), 1–10. https://doi.org/10.1016/j.fuel.2016.10.021
30. Y. Lan, D. Li, R. Yang, W. Liang, L. Zhou, Z. Chen, Computer simulation study on the compatibility of cyclotriphosphazene containing aminopropylsilicone functional group in flame retarded polypropylene/ammonium polyphosphate composites, *Compos. Sci. Technol.*, **88** (2013), 9–15. https://doi.org/10.1016/j.compscitech.2013.08.026
31. H. Wang, Z. You, J. Mills-Beale, P. Hao, Laboratory evaluation on high temperature viscosity and low temperature stiffness of asphalt binder with high percent scrap tire rubber, *Constr. Build. Mater.*, **26** (2012), 583–590. https://doi.org/10.1016/j.conbuildmat.2011.06.061

32. Y. Qiao, W. Sheng, C. He, C. Liu, Z. Rao, Experimental study on the effect of different surfactants on the thermophysical properties of graphene filled nanofluids, *Int. J. Energy Res.*, **45** (2021), 10043–10063. https://doi.org/10.1002/er.6497
33. Y. Meng, H. Guo, R. Xu, L. Liu, Study on the properties of graphene modified rubber asphalt under the effect of thermal aging, *Gongneng Cailiao/Journal Funct. Mater.*, **51** (2020), 08001–08006. https://doi.org/10.3969/j.issn.1001-9731.2020.08.001
34. S. D. Christian, Regular and related solutions: The solubility of gases, liquids, and solids(Hildebrand, Joel H; Prausnitz, John M.), *J. Chem. Educ.*, **48** (1971), 562–A562. https://doi.org/10.1021/ed048pa562.1
35. Z. Long, L. You, X. Tang, W. Ma, Y. Ding, F. Xu, Analysis of interfacial adhesion properties of nano-silica modified asphalt mixtures using molecular dynamics simulation, *Constr. Build. Mater.*, **255** (2020), 119354. https://doi.org/10.1016/j.conbuildmat.2020.119354
36. C. Li, S. Fan, T. Xu, Method for evaluating compatibility between SBS modifier and asphalt matrix using molecular dynamics models, *J. Mater. Civ. Eng.*, **33** (2021), 4021207. https://doi.org/10.1061/(asce)mt.1943-5533.0003863
37. R. Yu, C. Fang, P. Liu, X. Liu, Y. Li, Storage stability and rheological properties of asphalt modified with waste packaging polyethylene and organic montmorillonite, *Appl. Clay Sci.*, **104** (2015), 1–7. https://doi.org/10.1016/j.clay.2014.11.033
38. A. H. Abed, H. U. Bahia, Enhancement of permanent deformation resistance of modified asphalt concrete mixtures with nano-high density polyethylene, *Constr. Build. Mater.*, **236** (2020), 117604–117604. https://doi.org/10.1016/j.conbuildmat.2019.117604
39. C. Yu, K. Hu, Q. Yang, D. Wang, W. Zhang, G. Chen, et al., Analysis of the storage stability property of carbon nanotube/recycled polyethylene-modified asphalt using molecular dynamics simulations, *Polymers (Basel)*, **13** (2021), 1658–1658. https://doi.org/10.3390/polym13101658
40. Q. Zeng, Y. Liu, Q. Liu, P. Liu, Y. He, Y. Zeng, Preparation and modification mechanism analysis of graphene oxide modified asphalts, *Constr. Build. Mater.*, **238** (2020), 117706. https://doi.org/10.1016/j.conbuildmat.2019.117706
41. X. Zhang, G. Huang, C. Zhou, X. Yuan, J. He, M. Feng, et al., Research status of graphene material in fields of asphalt composites, *Zhongnan Daxue Xuebao (Ziran Kexue Ban)/Journal Cent. South Univ. (Science Technol.*, **50** (2019), 1637–1644. https://doi.org/10.11817/j.issn.1672-7207.2019.07.017
42. L. Gong, R. J. Young, I. A. Kinloch, I. Riaz, R. Jalil, K. S. Novoselov, Optimizing the reinforcement of polymer-based nanocomposites by graphene, *ACS Nano*., **6** (2012), 2086–2095. https://doi.org/10.1021/nn203917d
43. Y. Q. Tan, G. N. Li, L. Y. Shan, H. J. Lyu, A. X. Meng, Research progress of bitumen microstructures and components, *Jiaotong Yunshu Gongcheng Xuebao/J. Traffic Transp. Eng.*, **20** (2020). https://doi.org/10.19818/j.cnki.1671-1637.2020.06.001

AIMS Press